Molecularly Imprinted Polymer–decorated Magnetite Nanoparticles for Selective Sulfonamide Detection

Alejandro Zamora-Gálvez[†,§], Abdellatif Ait-Lahcen[†,‡,§], Luiza A. Mercante[†,ǁ], Eden Morales-Narváez[†], Aziz Amine[‡], Arben Merkoçi[†,ǂ,*]

[†]Catalan Institute of Nanoscience and Nanotechnology (ICN2), CSIC and The Barcelona Institute of Science and Technolgy, Campus UAB, Bellaterra, 08193 Barcelona, Spain

[‡]Faculty of Science and Technology, University Hassan II of Casablanca, B.P.146, 20650, Mohammedia, Morocco.

[ǁ]National Laboratory for Nanotechnology in Agribusiness (LNNA), Embrapa Instrumentation, 13560-970, São Carlos, SP, Brazil

[ǂ]ICREA – Catalan Institution for Research and Advanced Studies, Barcelona, 08010, Spain

ABSTRACT: Sulfonamides are known not only to be antimicrobial drugs, which lead to antimicrobial resistance, but also to be chemotherapeutic agents that may be allergenic and potentially carcinogenic, which represent a potentially hazardous compound once being present in soil or water. Herein, a hybrid material based on molecularly imprinted polymer (MIP)–decorated magnetite nanoparticles for specific and label-free sulfonamide detection is reported. The composite has been characterized using different spectroscopic and imaging techniques. The magnetic properties of the composite are used to separate, pre-concentrate, and manipulate the analyte which is selectively captured by the MIP onto the surface of the composite. Screen printed electrodes have been employed to monitor the impedance levels of the whole material, which is related to the amount of the captured analyte, via electrochemical impedance spectroscopy. This composite-based sensing system exhibits an extraordinary limit of detection of 1×10^{-12} mol L^{-1} (2.8×10^{-4} ppb) (S/N = 3), which is close to those obtained with liquid chromatography and mass spectrometry, and it was demonstrated to screen sulfamethoxazole in a complex matrix such as seawater, where according to the literature sulfonamides content is minimum compared with other environmental samples.

Since the mid-twentieth century, sulfonamides have been extensively exploited as antimicrobial agents in humans and animals.[1–3] On the one hand, it is well-known that the use of antibiotics leads to antimicrobial resistance, which is an international serious concern.[4] On the one hand, sulfonamides have been reported not only to elicit dermatological eruptions,[5] but also to be potentially carcinogenic among other health consequences.[2,3] On the other hand, medical treatments, livestock and aquaculture operations of an exponentially growing human population have a great demand for sulfonamides compounds, which may reach the environment through wastewater from pharmaceutical or food chains involving human and animal waste. In fact, it is estimated that every year more than 20 thousand tons of sulfonamides reach the global environment.[1] Therefore, as a potential health threat, highly sensitive monitoring of sulfonamide residues is relevant to enforce food safety and environmental quality.

Dmitrienko et al. have recently performed a broad study on the recent trends towards sulfonamides detection.[1] Sulfonamide residues are generally screened using time-consuming but highly sensitive, robust and reliable methods involving complex apparatus operated by skilled personnel; for instance, liquid chromatography,[6,7] mass spectrometry[8,9]or capillary electrophoresis.[10,11] Consequently, alternative antibiotic residues screening methods such as immunoassays and biosensing platforms are rising considerably.[3] These alternatives are leading to a promising analytical performance in terms of sensitivity; for example, they bear limits of detection of up to 5×10^{-2} ppb.[1] However, they have not been reported to be as sensitive and have limits of detection as those achieved by solid-phase extraction working in synergy with liquid chromatography/mass spectrometry, which has been reported to be up to 9×10^{-5} ppb.[1]

Biosensing technology incorporates biorecognition elements integrated with a transducing system that leads to a specific signal upon analyte recognition. The signal can be optical, electrochemical or mechanical among others; whereas enzymes, antibodies, oligonucleotides or other biomolecules can be exploited as biorecognition elements. However, biosensing technology is also taking advantage of biomimetic recognition elements such as molecularly imprinted polymers (MIPs),[12,13] for example when biorecongition elements targeting small molecules are technically difficult to obtain.[14] MIPs are synthetic polymers typically obtained by copolymerization of a monomer with a cross-linker in the presence of a template molecule.[15] The shape, size, and functionalities of MIPs are complementary to the target analyte, which is used as template molecule. Consequently, they can selectively recognize and bind specific target molecules through non-covalent strength interactions between the host matrix and the guest molecule, including Van der Waals force, hydrogen bonding, electrostatic features, hydrophobic phenomena and metal-ion coordination.[16]

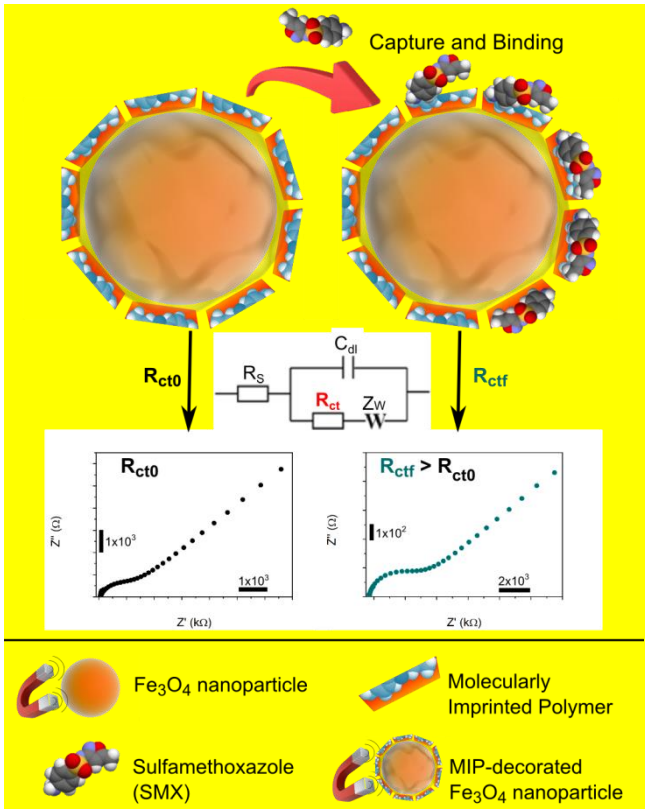

Figure 1. Schematic representation of the proposed nano-enabled sensing system. The proposed system operates via electrochemical impedance spectroscopy. Abbreviations: R_s is the electrolyte resistance, C_{dl} is the interface capacitance, R_{ct} is the charge (electron) transfer resistance and Z_w is the Warburg impedance.

Herein, a composite material based on molecularly imprinted polymer (MIP) and Fe_3O_4 superparamagnetic nanoparticles (MNPs) that is designed to specifically detect sulfamethoxazole[17–21] (SMX) with extraordinary sensitivity is reported. Scanning electron microscopy (SEM), transmission electron microscopy (TEM), X-ray photoelectron spectroscopy (XPS) and Fourier transform infrared spectroscopy (FT-IR) have been utilized to characterize the proposed hybrid material. The superparamagnetic properties of the composite are utilized to pre-concentrate, separate and manipulate the analyte which is selectively captured by the MIP onto the surface of the composite. On the other hand, disposable screen printed electrodes, have been used to monitor the impedance levels of the whole material, which is related to the amount of the captured analyte via electrochemical impedance spectroscopy, facilitating a simple and label-free sensing platform (see Figure 1).

EXPERIMENTAL

Chemicals and Materials.

Sulfamethoxazole, sulfadiazine, sulfacetamide, dimethyl sulfoxide, acetic acid, methacrylic acid, iron chloride (II), iron chloride (III), ammonium hydroxide, polyvinylpyrrolidone, oleic acid, 2,5-Bis(tertbutylperoxy)-2,5dimethylhexane, potassium hexacyanoferrate (II) and potassium hexacyanoferrate (III) were purchased from Sigma Aldrich (Madrid, Spain). Methanol was purchased from Labbox (Vilassar de Dalt, Barcelona, Spain). Stock solutions of sulfamethoxazole, sulfadiazine and sulfacetamide were prepared in methanol/water (1:1, v/v). Seawater samples were extracted from Poblenou Beach (Barcelona, Spain). Seawater samples were filtered using filter paper and then a nitrocellulose membrane (0.025 μm, Millipore, Billerica, Massachusetts, USA).

TEM analysis was performed using a FEI TECNAI G2 F20 (Hillsboro, Oregon, USA). XPS analysis was carried out with a Phoibos 150 analyser (SPECS GmbH, Berlin, Germany) in ultra-high vacuum conditions ($1x10^{-10}$ mbar) with a monochromatic aluminium K-alpha (Kα) X-ray source (1486.74 eV). The energy resolution (0.58 eV) was measured by the full width at half-maximum intensity of the Ag $3d^{5/2}$ peak for a sputtered silver foil. SEM analysis was performed using a FEI Magellan (Hillsboro, Oregon, USA) and FT-IR analysis was carried out by IR-ATR (attenuated total reflectance) for direct measuring, model IR Tensor 27 (Bruker, Billerica, Massachusetts, USA). A computer-controlled Autolab PGSTAT-12 (302N-High performance) (potentiostat/galvanostat) with a general purpose electrochemical impedance software operating system (Frequency Response Analysers, FRA, v.4.9.006, Solartron Metrology, Leicester, England) was used for impedance measurements. BET (Brunauer-Emmett-Teller) measurements were performed with an ASAP-2000 instrument from Micromeritics and were carried out for N_2 relative vapor pressure of 0.05−0.3 at 77 K.

Screen printed carbon electrodes (SPCE)

The SPEs consist of a single plastic strip containing three electrodes: working, reference and counter electrode. They were produced by screen-printed technology using a screen-printed machine (DEK 248). Masks galvanized steel frames (580 x 580 x 35 x 25 mm) with 4xM6 holes (Pantur ,Sabadell, Spain), photolithograph masks (P1000 + ENT5060P110 Entelar 54 x 58 P-110 + INDZ5060 Exposure diazo 54 x 58, Paimser, Cerdañola del Valles, Spain), polyester substrate (Autostat HT5, McDermid Autotype, UK) and thermostatic oven (J.P Selecta, Abrera, Barcelona, Spain) were also utilized. Three different inks were used: graphite ink for the working and counter electrode (Electrodag 423SS ink), silver/silver chloride for the reference electrode layer (Electrodag 6037SS ink) and finally an insulating layer (Minico M-7000 Blue) to define the working electrode area and avoid the undesirable contacts of the liquid with the internal connections. All the inks were purchased from Gwent Group, (Mamhilad Pk Est, Pontypool, UK). The fabrication procedure involves three printing process. In the first process the graphite layer was printed onto a polyester sheet by using the first stencil and the graphite ink. After this, the ink was cured at 60 °C for 15 minutes. The silver ink layer was printed and cured at the same conditions, to be used as the reference electrode. Then, an insulating ink printing process was carried out. After this step the SPEs were stored in dry environment prior to be used. It is noteworthy that the graphite ink, C2030519P4, is a conductive screen printable ink containing carbon nanoparticles dispersed in a thermoplastic resin.

Synthesis of magnetite nanoparticles

Magnetite nanoparticles were prepared by co-precipitation method,[22–25] mixing 0.05 mol of $FeCl_3 \cdot 6H_20$ and 0.025 mol $FeCl_2 \cdot 4H_20$ in 250 mL of ultrapure water, using a 500 mL three neck flask. The mixture was stirred under nitrogen atmosphere and heated until 80ºC, and then 20 mL of NH_4OH from the stock solution, was added (drop by drop). The reaction remained under reflux for 40 min and was cooled down at room temperature. The black product was separated and washed with ultrapure water three times. Lastly, the product was dried under

vacuum at 45ºC. In order to evaluate the influence of the nanoparticles size on the sensing properties of MIPs, bigger magnetite nanoparticles were also synthesized following the same experimental conditions, but changing the molar ratio between Fe^{2+}/Fe^{3+} from 1:2 to 1:0.25.[26,27]

Synthesis of molecularly imprinted polymer-decorated magnetite nanoparticles

To synthesize the MIP-decorated MNPs for SMX detection, two solutions were prepared. Firstly, 1 mL of sulfametoxazole (10 mmol) was solubilized with 10 mL of DMSO and 4 mmol of methacrylic acid (MAA) and the solution was stirred for 30 min. Fe_3O_4 MNPs were mixed with 1 mL of oleic acid and 10 mmol of pyrrole (Py). Secondly, the solution made of DMSO, MAA and SMX was added to the Fe_3O_4 MNPs/Py solution and immersed in an ultrasound bath for 30 min. Under nitrogen atmosphere, 150 mL of DMSO/water (9:1, v/v), 1g of PVP (polyvinylpyrrolidone), the Fe_3O_4 MNPS/Py/SMX solution and 0.3 mmol of radical initiator (2,5-Bis(tertbutylperoxy)-2,5 dimethylhexane) were added in a two neck flask. The mixture was allowed to react for 24 h at 60ºC. The final product was separated and washed with a mixture of methanol/acetic acid (4:1, v/v) and purified using a Soxhlet extractor with methanol/water (1:1, v/v), and dried under vacuum. The non-imprinted polymer (NIP) was synthesized using the same method in the absence of the analyte (SMX).

Binding experiments

A range of different concentrations of SMX, starting from $1x10^{-2}$ mol L^{-1} until $1x10^{-10}$ mol L^{-1} was prepared in a mixture of methanol and water (1:1, v/v), and then 20 mg of MIP-decorated Fe_3O_4 MNPs was added into each sample. The solutions were incubated for 2 hours at 700 rpm. After that, three successive centrifugation processes were made during 5 min at 10000 rpm, removing the supernatant and replacing the solvent with new methanol/water solution. The final solution was reconstituted in ultrapure water. Seawater samples were collected from Barcelona Mediterranean Sea (Poblenou Beach) and treated through filtration to remove potential interfering species contained within the original matrix. Various seawater sample solutions containing SMX with concentrations from $1x10^{-2}$ to $1x10^{-10}$ mol L^{-1} were prepared by spiking method. Then, 0.5 mL of extraction media (methanol/acetic acid 1:1, v/v) was added in each sample in order to extract interfering compounds presents in the matrix of the sample, and incubated for 10 min at 650 rpm. In each pre-treated sample to be analyzed, 20 mg of MIP-decorated Fe_3O_4 MNPs was added, and then 2-hour incubation was performed at 25ºC and 700 rpm. Finally in order to remove the template, a centrifugation step was done. Three successive centrifugations were carried out, each one during 5 min at 10000 rpm, removing the supernatant and replacing for methanol/water solution. The final solution was reconstituted in 2 mL ultrapure water. The electroanalytical performance of the proposed sensing system was investigated using electrochemical impedance spectroscopy (EIS). The measurements were performed using home-made screen printed carbon electrodes (SPCE) and 1 mmol L^{-1} $[Fe(CN)_6]^{3-/4-}$ with 0.1 mol L^{-1} KCl as redox probe. MIP-decorated MNPs were fixed over the working electrode using a magnet underneath the SPCE to perform impedance measurements. The resulting data was fitted in a regular Randles circuit to extract the value of charge transfer resistance (R_{ct}) using FRA (v.4.9.006) software.

RESULTS AND DISCUSSION

Characterization of Fe_3O_4 MNPs and MIP-decorated Fe_3O_4 MNPs

Fe_3O_4 MNPs and MIP-decorated Fe_3O_4 MNPs were first characterized by TEM. As shown in Figure 2A, the magnetite nanoparticles have a sphere-like shape and an average size of 11 ± 2 nm (Figure S1A). After being coated with the MIP, due to the polymerization process, the resulted MIP-decorated Fe_3O_4 MNPs were observed to be arranged in clusters with an average diameter of 30-50 nm (Figure 2B and Figure S1B), suggesting that the MIP was successfully deposited onto the surface of the nanoparticles.

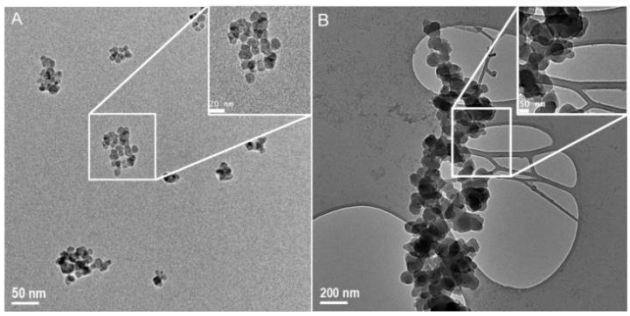

Figure 2. TEM images of (A) Fe_3O_4 MNPs and (B) MIP-decorated Fe_3O_4 MNPs.

Aiming at confirming the composition of the synthetized materials, XPS analysis was performed. The spectrum presented in Figure 3A shows two peaks at 711 and 725 eV corresponding to $Fe2p_{3/2}$ and $Fe2p_{1/2}$. The Fe2p doublet peaks involve the presence of typical magnetite Fe–O bonds, confirming the formation of the magnetite. The spectra of the MIP-decorated Fe_3O_4 MNPs (Figure 3B) do not display the iron signals; this is probable due to the fact that the polymeric layer surrounding the magnetite exceeds the maximum depth that XPS can analyze (around 20 nm). Knowing that, it is possible to see on Figure 3B the signal for C_{1s} at 277 eV, corresponding to C-C signal, and another smaller peak at 281eV, related to the C-O-C bond from the different compounds used in the synthesis process. The peaks at 525 eV and 392 eV are ascribed to O_{1s} and N_{1s}, respectively.

FT-IR experiments were also carried out to investigate the formation of MIP-decorated Fe_3O_4 MNPs. Figure 3C shows the FT-IR spectra of Fe_3O_4 MNPs (black line) and MIP-decorated Fe_3O_4 MNPs (red line). Fe_3O_4 MNPs display a main absorption band at 539 cm^{-1} assigned to Fe−O stretching. Regarding the spectra of MIP-decorated Fe_3O_4 MNPs, it is possible to observe a broad band centered at 3300 cm^{-1} ascribed to the stretching vibration of −OH and–NH groups from the methanol. The peaks at 1636 cm^{-1} and 949 cm^{-1} are related to C=C from the pyrrole aromatic ring. The multiple peaks from 1457 to 1320 belong to the pyrrole backbone ring. The peak at 3400 cm^{-1} corresponds to N-H, the peak 1248 cm^{-1} corresponds to C-N, and the peak at 1145 cm^{-1} is ascribed to S=O bonds, these groups belongs to sulfamethoxazole (see figure S2). These results confirm that the MIP was successfully imprinted on the surface of the Fe_3O_4 MNPs.

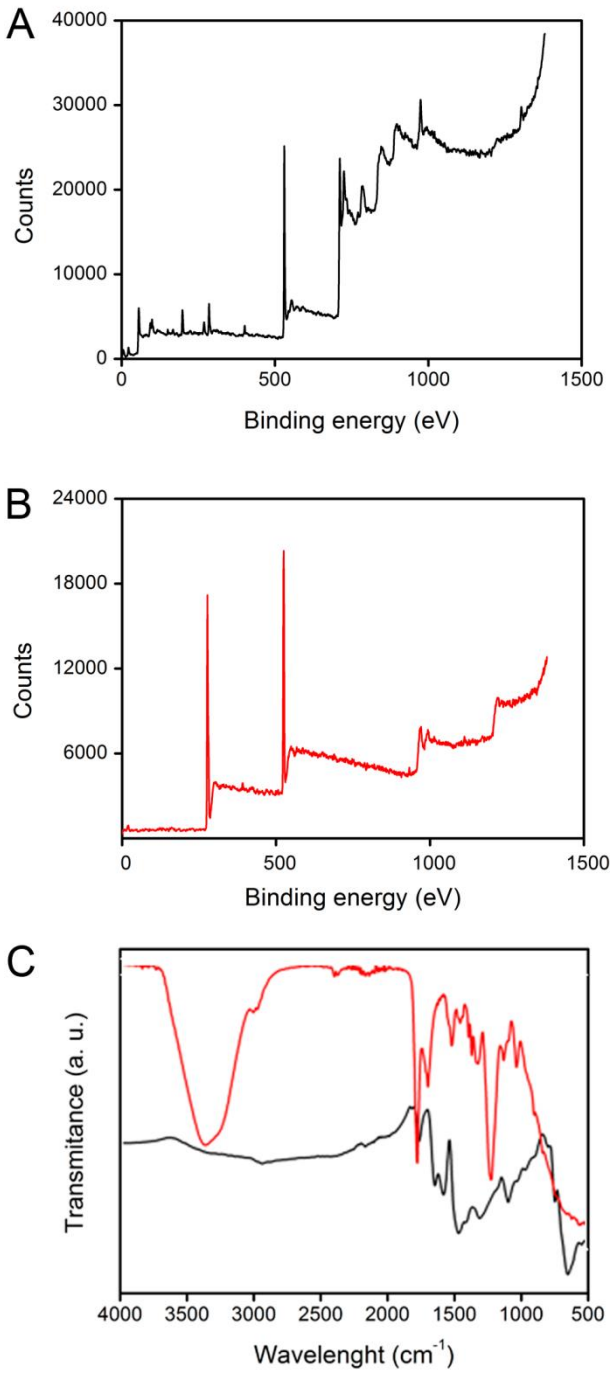

Figure 3. X-ray photoelectron spectroscopy, (A) Fe_3O_4 MNPs, (B) MIP-decorated Fe_3O_4 MNPs and (C) FTIR spectra of Fe_3O_4 MNPs (black line) and MIP-decorated Fe_3O_4 MNPs (red line).

Electrochemical impedance responses of the MIP-decorated Fe_3O_4 MNPs toward SMX

Electrochemical impedance spectroscopy (EIS) is an effective tool to analyze changes that take place at an interface during a recognition event.[28] In brief, EIS measurements can be performed in two ways: Faradaic EIS and non-Faradaic method. Faradaic impedance measurements are usually carried out by using a reversible redox probe while non-Faradaic impedance measurements are done without using any redox probe.[29,30] Both Faradic [31,32] and non-Faradic [33,34] impedance spectroscopy have been applied for the studies of the recognition events involved in MIP. Importantly, improved sensitivity has been reported for Faradaic measurements.[30] The typical impedance data are presented in the form of the Nyquist plot and relies on a semicircular region at higher frequencies corresponding to the interfacial charge-transfer process and a linear part at lower frequency range representing the diffusion process. The semicircle diameter in the Nyquist plot corresponds to the charge transfer resistance (R_{ct}), which reflects the electron-transfer kinetics of the redox probe at the electrode surface.[29] In this work, Faradaic EIS measurements were performed through SPCEs in a 1 mmol L^{-1} $[Fe(CN)_6]^{3-/4-}$ solution containing 0.1 mol L^{-1} KCl using a potential of 0.24 V over the frequency range from 0.1 Hz to 100 kHz and a voltage amplitude of 50 mV. Comprising MIP-decorated Fe_3O_4 MNPs was carried out in ultrapure water in the absence and presence of different concentrations of SMX (from 1×10^{-2} mol L^{-1} to 1×10^{-10} mol L^{-1}) in the frequency range from 0.1 Hz to 100 kHz (Figure 4). The obtained results were analyzed using a Randles equivalent circuit (see Figure 4 inset *i*), where: R_s is the electrolyte resistance, C_{dl} is the interface capacitance, R_{ct} is the charge (electron) transfer resistance and Z_w is the Warburg impedance. Different R_{ct} values were obtained for each SMX concentration. The R_{ct} of the electrode in the absence of SMX is 68 **Ω**; this relatively small R_{ct} value can be attributed to the free electron transfer from the electrode surface to the solution.[30] The R_{ct} value increases due to the presence of the analyte, as the SMX molecule present in the solution gets bound via the recognition sites or cavities of the MIP. The magnitude of the change in R_{ct} increases as a function of SMX concentration in a logarithmic way in a wide range between 1×10^{-2} mol L^{-1} to 1×10^{-10} mol L^{-1}, as displayed in the inset. The linear regression equation was adjusted to R_{ct} (kΩ) = 0.01 log [SMX] (mol L^{-1}) + 0.31 (R^2 = 0.98), with an estimated detection limit of 1×10^{-12} mol L^{-1} (2.8×10^{-4} ppb), calculated as the concentration of SMX corresponding to the 3 times "*S/N*" ratio, where "*S*" is the standard deviation of the blank impedance signal (three replicates) and "*N*" is the slope of the related calibration curve. This sensing platform offers an advantageous performance in terms of limit of detection when compared to other methods for SMX determination (see Table 1).

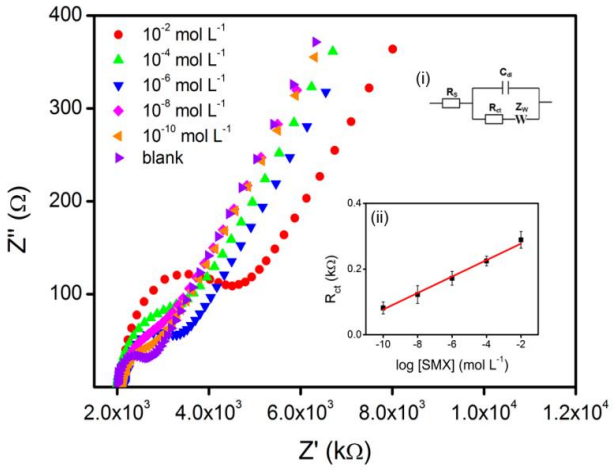

Figure 4. Nyquist plots of EIS of MIP-decorated Fe_3O_4 MNP-modified SPCE electrode in the presence of different SMX concentrations. EIS measurements were performed in a 1 mmol L^{-1} $[Fe(CN)_6]^{3-/4-}$ containing 0.1 mol L^{-1} KCl at a potential of 0.24 V over the frequency range from 0.1 Hz to 100 kHz, using a voltage amplitude of 50 mV. The insets are related to: (i) the Randles equivalent circuit model for the impedance data and (ii) the calibration curve obtained by plotting the R_{ct} values *vs* log

of SMX concentration in the range of 1 x 10^{-2} mol L^{-1} to 1 x 10^{-10} mol L^{-1}.

Table 1. Comparison of Composition, Detection Limit and Linear Range of Different Modified Electrodes for Determination of SMX

Method	Detection Limit	Linear range	Reference
MMIP (Fe_3O_4)	1.5 ng g^{-1}	1.5 - 4.3 ng g^{-1}	17
MIP-OPPy[a]	3.59 x 10^{-4} mM	25 x 10^{-3} - 0.75 mM	18
MIP-EDMA[b]	3.0 x 10^{-7} mol L^{-1}	3.0 x 10^{-7} - 4.0 x 10^{-4} mol L^{-1}	19
Broad specific immunoassay	65.2 µg L^{-1}	0.2 - 65.2 µg L^{-1}	20
LC-MS	5–10 ng g^{-1}	50 - 200 ppb	21
MIP-decorated Fe_3O_4 MNPs	1 x 10^{-12} mol L^{-1}	1 x 10^{-2} - 1 x 10^{-10} mol L^{-1}	This work

[a] OPPy - Overoxydized polypyrrole.

[b] EDMA - Ethylene glycol dimethacrylat.

The electrode reproducibility and stability were also investigated by impedimetric responses of sample solutions containing 10^{-6} mol L^{-1} SMX. The relative standard deviations (RSDs) of the same sensor for five successive measurements were found to be 3.6% and for three different electrodes it was 6.8%. These results confirm the electrode reproducibility. The imprinted sensor also exhibited satisfactory stability. In fact, the results show that after 3 weeks 82% of the initial response was preserved.

Characterization of the NIP-composite and selectivity studies

To confirm the specificity of the MIP-decorated Fe_3O_4 MNPs, its performance was compared with the performance of a non-imprinted polymer (NIP)-composite.[31–33] Figure 5A shows the R_{ct} values obtained for both materials in the absence and presence of 1 x 10^{-2} mol L^{-1} SMX. The difference observed on R_{ct} values for the imprinted sensor (160 Ω) and non-imprinted sensor (110 Ω) is related to the imprinted cavities presented on the MIP-composite, which facilitate the diffusion of the $[Fe(CN)_6]^{3-/4-}$ probes into the electrode surface, decreasing the charge transfer resistance.[34] Analyzing the Rct values corresponding to the sample containing SMX, the MIP-composite shows a value that is 3 times higher than the blank, whereas the NIP-composite displays a value that is 1.4 times higher than the blank. These large separation factors suggest that the MIP-composite possesses a high specificity towards SMX when compared with the NIP-composite behavior.

Interferences of other sulfonamides were also studied aiming at exploring the selectivity of the sensing system based on the proposed MIP-decorated Fe_3O_4 MNPs. In particular, the performance of the sensing system was evaluated in the presence of two kinds of structurally similar sulfonamides such as sulfadiazine (SDZ) and sulfacetamide (SCT). In a typical experiment, the electrochemical impedance of the electrode modified with the composite was measured in the presence of 1x10^{-8} mol L^{-1} of each analyte. As shown in Figure 5B, the R_{ct} values obtained for SDZ and SCT show practically no difference between them and the blank. These results suggest that the sensor exhibits good selectivity, which is attributed to the specificity of the MIP toward SMX.

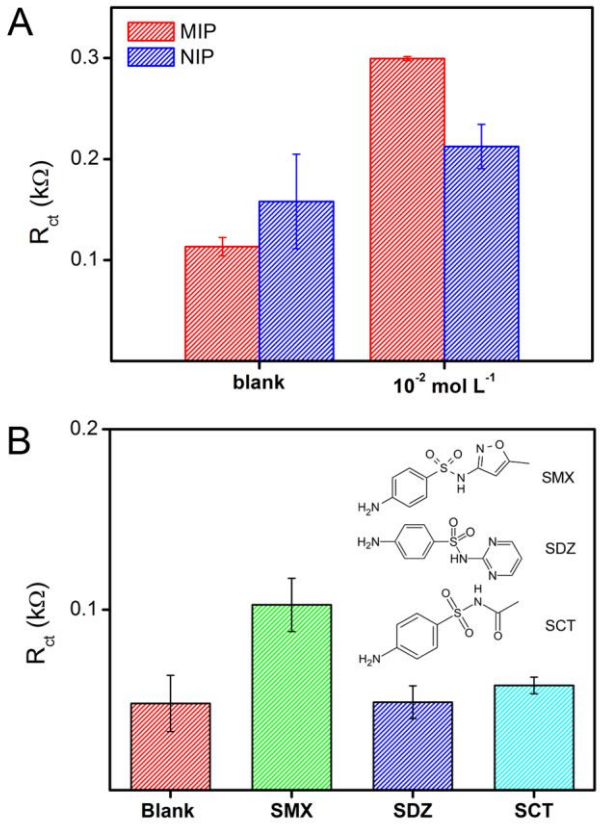

Figure 5. R_{ct} values obtained for (A) imprinted (MIP) and non-imprinted (NIP) sensor and (B) the MIP-decorated Fe_3O_4 MNPs in the presence of SMX, SDZ and SCT. Results obtained from the EIS measurements performed in a 1 mmol L^{-1} $[Fe(CN)_6]^{3-/4-}$ containing 0.1 mol L^{-1} KCl at a potential of 0.24 V over the frequency range from 0.1 Hz to 100 kHz, using a voltage amplitude of 50 mV.

Real sample analysis

In order to evaluate the applicability of the proposed sensor in real environmental samples, determination of SMX was carried out in spiked seawater samples. Prior to the analysis, the samples were mixed with extraction media (see experimental description) in order to minimize matrix complexity and spike the samples with different SMX concentrations. It was observed from the EIS data (Figure 6) that the R_{ct} value increased on spiking with SMX. Hence, from the R_{ct} values obtained for three different SMX concentrations (10^{-4}, 10^{-6} and 10^{-8} mol L^{-1}), recovery was calculated and the results obtained are given in Table 2. The recoveries of the samples are 87 - 106 % with the RSD in the range of 1.2 - 4.5 %, which indicates that the developed assay can be performed for the accurate determination of SMX in real samples analysis.

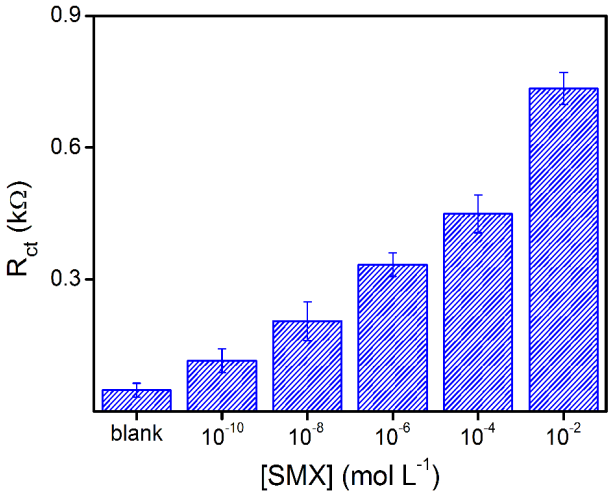

Figure 6. R_{ct} values obtained for MIP-decorated Fe_3O_4 MNPs in seawater in the absence and presence of different spiked SMX concentrations. Results obtained from the EIS measurements performed in a 1 mmol L^{-1} $[Fe(CN)_6]^{3-/4-}$ containing 0.1 mol L^{-1} KCl at a potential of 0.24 V over the frequency range from 0.1 Hz to 100 kHz, using a voltage amplitude of 50 mV.

Table 2. Determination of SMX in seawater.

SMX Spiked (mol L^{-1})	Rct (kΩ)	Recovery (%)	RSD (%)
10^{-4}	0.233	92	1.2
10^{-6}	0.174	87	4.5
10^{-8}	0.115	106	2.3

Fe_3O_4 MNPs size effect study

MIP-composite was also synthesized using bigger magnetite nanoparticles. The new magnetite nanoparticles were characterized using TEM, which shows the formation of nanoparticles with diameter around 27 nm (Figure S3A). Binding experiments for the new MIP was carried out following the same procedure. From the EIS data obtained for the composite containing Fe_3O_4 MNPs of 27 nm, a new calibration curve was constructed (Figure S3B) and a new limit of detection was also determined (S/N = 3). The LOD for the new MIP-composite shows a different performance when compared with that of the original one, obtaining 5 x 10^{-12} mol L^{-1} (1.4 x 10^{-3} ppb), being 5 times higher than that obtained with the composite based on particles of an average diameter of 11 nm (1 x 10^{-12} mol L^{-1}).

Since the new-proposed sensing system was found to offer a different performance in terms of limit of detection by changing the size of the particles embedded in the composite, the specific surface area of both composites was explored via Brunauer-Emmett-Teller (BET) technique in order to verify the influence of this parameter in the limit of detection of the developed sensing system. Hence, the limit of detection of the proposed sensing system using the MIP-decorated Fe_3O_4 MNPs containing two different sizes of particles, 11 and 27 nm respectively, was systematically studied in parallel with the BET analysis (Figure S4). The composite decorated with 27 nm Fe_3O_4 NPs showed a surface area of 64 m^2g^{-1}, whereas the composite of 11 nm displayed a larger surface area of 184 m^2g^{-1} due to the smaller size of MNPs. From this data, it can be concluded that smaller nanoparticles can improve the surface area, increasing the number of the recognition sites for SMX which improves the electrochemical response of the sensing system. Table 3 summarizes the obtained results.

Table 3. The influence of the specific surface area on the limit of detection of the proposed sensing system.

Particle size (nm)	LOD (mol L^{-1})[a]	SSA (m^2 g^{-1})[b]
11	1 x 10^{-12}	64
27	5 x 10^{-12}	184

a. Limit of detection (S/N = 3), b. Specific surface area

CONCLUSIONS

A selective, specific and highly sensitive composite-based sensing system has been engineered aiming at detecting the potentially hazardous chemotherapeutic agent SMX in a label-free fashion via electrochemical impedance spectroscopy. The proposed sensing system (i) bears selectivity and specificity, due to its biomimetic receptor; (ii) facilitates pre-concentration, separation and manipulation of the analyte, due to its magnetic properties; (iii) showing a high surface area (184 m^2 g^{-1}), this composite-based sensing system exhibits a high sensitivity (LOD around 1 x 10^{-12} mol L^{-1} ≈ 2.8 x 10^{-4} ppb), which is comparable with that of sulfonamides monitoring using liquid chromatography/mass spectrometry. Moreover, this sensing system has been proved to be useful in seawater monitoring, where sulfonamides content is minimum compared to other environmental samples and may be extended to other compounds by changing the MIP.

ASSOCIATED CONTENT

Supporting Information

Sizes distributions Fe_3O_4 MNPs MIP-decorated Fe_3O_4 MNPs, detailled FT-IR, TEM image and size distribution of 27nm-Fe_3O_4 MNPs, Calibration curve for the MIP-composite based on particles of an average diameter of 27 nm and N2 adsorption isotherms. This material is available free of charge on the ACS Publications website.

AUTHOR INFORMATION

Corresponding Author

* Arben Merkoçi, arben.merkoçi@icn.cat

Author Contributions

§ These authors contributed equally to this work.

ACKNOWLEDGMENT

This work was supported by: The European Commission Program, FP7-OCEAN, SMS Project (613844). ICN2 acknowledges support from the Severo Ochoa Program (MINECO, Grant SEV- 2013-0295). Nanobiosensors and Bioelectronics Group acknowledges Supramolecular NanoChemistry and Materials group (Dr. Carlos Carbonell and Prof. Daniel Maspoch at ICN2) for BET measurements, and the support from Secretaria d'Universitats i Recerca del Departament d'Economia i Coneixement de la Generalitat de Catalunya (2014 SGR 260). L.A.M acknowledges financial support from FAPESP-BEPE (2014/26088-4) project.

REFERENCES

(1) Dmitrienko, S. G.; Kochuk, E. V; Apyari, V. V; Tolmacheva, V. V; Zolotov, Y. A. *Anal. Chim. Acta* **2014**, *850*, 6–25.
(2) Wang, S.; Zhang, H. Y.; Wang, L.; Duan, Z. J.; Kennedy, I. *Food Addit. Contam.* **2006**, *23* (4), 362–384.
(3) Cháfer-Pericás, C.; Maquieira, Á.; Puchades, R. *TrAC Trends Anal. Chem.* **2010**, *29* (9), 1038–1049.
(4) O'Neill, J. *Rev. Antimicrob. Resist.* **2014**, No. December, 1–16.
(5) Meltzer, L. *J. Invest. Dermatol.* **1949**, *13* (4), 213–216.
(6) Hela, W.; Brandtner, M.; Widek, R.; Schuh, R. *Food Chem.* **2003**, *83* (4), 601–608.
(7) Nebot, C.; Regal, P.; Miranda, J. M.; Fente, C.; Cepeda, A. *Food Chem.* **2013**, *141* (3), 2294–2299.
(8) Lindsey, M. E.; Meyer, T. M.; Thurman, E. M. *Anal. Chem.* **2001**, *73* (19), 4640–4646.
(9) Rodriguez, M.; Orescan, D. B. *Anal. Chem.* **1998**, *70* (13), 2710–2717.
(10) Fuh, M. R. S.; Chu, S. Y. *Anal. Chim. Acta* **2003**, *499* (1-2), 215–221.
(11) Santos, B.; Lista, A.; Simonet, B. M.; Ríos, A.; Valcárcel, M. *Electrophoresis* **2005**, *26* (7-8), 1567–1575.
(12) Merkoçi, a.; Alegret, S. *TrAC Trends Anal. Chem.* **2002**, *21* (11), 717–725.
(13) Schirhagl, R. *Anal. Chem.* **2014**, *86* (1), 250–261.
(14) Zor, E.; Morales-Narváez, E.; Zamora-Gálvez, A.; Bingol, H.; Ersoz, M.; Merkoçi, A. *ACS Appl. Mater. Interfaces* **2015**, *7* (36), 20272–20279.
(15) Chantada-Vázquez, M. P.; Sánchez-González, J.; Peña-Vázquez, E.; Tabernero, M. J.; Bermejo, A. M.; Bermejo-Barrera, P.; Moreda-Piñeiro, A. *Biosens. Bioelectron.* **2016**, *75*, 213–221.
(16) Wan, Y.; Ma, H.; Lu, B. *Adv. Biochem. Eng. Biotechnol.* **2015**, *150*, 131–166.
(17) Chen, L.; Zhang, X.; Sun, L.; Xu, Y.; Zeng, Q.; Wang, H.; Xu, H.; Yu, A.; Zhang, H.; Ding, L. *J. Agric. Food Chem.* **2009**, *57* (21), 10073–10080.
(18) Ozkorucuklu, S. P.; Sahin, Y.; Alsancak, G. *Sensors* **2008**, *8* (12), 8463–8478.
(19) Guzm, A.; Prada, D.; Mart, P.; Reviejo, A. J.; Pingarr, J. M. **2005**, *539*, 125–132.
(20) Franek, M.; Diblikova, I.; Cernoch, I.; Vass, M.; Hruska, K. **2006**, *78* (5), 1559–1567.
(21) Heller, D. N.; Ngoh, M. A.; Donoghue, D.; Podhorniak, L.; Righter, H.; Thomas, M. H. **2002**, *774*, 39–52.
(22) Machala, L.; Zboril, R.; Gedanken, A. *J. Phys. Chem. B* **2007**, *111* (16), 4003–4018.
(23) Lee, Y.; Lee, Y.; Lee, J.; Lee, J.; Bae, C. J.; Bae, C. J.; Park, J.-G.; Park, J.-G.; Noh, H.-J.; Noh, H.-J.; Park, J.-H.; Park, J.-H.; Hyeon, T.; Hyeon, T. *Adv. Funct. Mater.* **2005**, *15* (3), 503–509.
(24) Prozorov, T.; Mallapragada, S. K.; Narasimhan, B.; Wang, L.; Palo, P.; Nilsen-Hamilton, M.; Williams, T. J.; Bazylinski, D. a.; Prozorov, R.; Canfield, P. C. *Adv. Funct. Mater.* **2007**, *17* (6), 951–957.
(25) Huynh, T.-P.; Wojnarowicz, A.; Sosnowska, M.; Srebnik, S.; Benincori, T.; Sannicolò, F.; Souza, F. D.; Kutner, W. *Biosens. Bioelectron.* **2015**, *70*, 153–160.
(26) Herea, D.-D.; Chiriac, H.; Lupu, N. *J. Nanoparticle Res.* **2011**, *13* (9), 4357–4369.
(27) Sun, S.; Zeng, H. *J. Am. Chem. Soc.* **2002**, *124* (28), 8204–8205.
(28) Mayorga-Martinez, C. C.; Chamorro-Garcia, A.; Merkoçi, A. *Biosens. Bioelectron.* **2015**, *67*, 53–58.
(29) Gautier C.; Esnault C.; Cougnon C.; Pilard J.; Casse N.; Chénais B.; *J. Electroanal. Chem.* **2007**, *610*. 227–233
(30) Patil, A. V.; Bedatty Fernandes, F. C.; Bueno, P. R.; Davis, J. J. *Anal. Chem.* **2015**, *87* (2), 944–950.
(31) Uygun, Z. O.; Dilgin, Y. *Sensors Actuators, B Chem.* **2013**, *188*, 78–84.
(32) Wu, B.; Wang, Z.; Zhao, D.; Lu, X. *Talanta* **2012**, *101*, 374–381.
(33) Apodaca, D. C.; Pernites, R. B.; Ponnapati, R.; Del Mundo, F. R.; Advincula, R. C. *Macromolecules* **2011**, *44* (17), 6669–6682.
(34) Reddy, K. K.; Gobi, K. V. *Sensors Actuators, B Chem.* **2013**, *183*, 356–363.
(35) Yao, G.; Liang, R.; Huang, C.; Wang, Y.; Qiu, J. **2013**.
(36) Reddy, K. K.; Gobi, K. V. *Sensors Actuators B Chem.* **2013**, *183*, 356–363.
(37) Nishad, P. A.; Bhaskarapillai, A.; Velmurugan, S.; Narasimhan, S. V. *Carbohydr. Polym.* **2012**, *87* (4), 2690–2696.
(38) Sergeyeva, T. A.; Piletsky, S. a.; Panasyuk, T. L.; El'skaya, a. V.; Brovko, a. a.; Slinchenko, E. a.; Sergeeva, L. M. *Analyst* **1999**, *124* (3), 331–334.
(39) Pan, G.; Zu, B.; Guo, X.; Zhang, Y.; Li, C.; Zhang, H. *Polymer (Guildf).* **2009**, *50* (13), 2819–2825.
(40) Zhu, L.; Cao, Y.; Cao, G. *Biosens. Bioelectron.* **2014**, *54*, 258–261.

For TOC only